Validation of an Acoustic Impedance Prediction Model for Skewed Resonators

Brian M. Howerton [1]
Lockheed-Martin Space and Science Solutions, Hampton, VA 23681-2199 USA

and

Tony L. Parrott[2]
NASA Langley Research Center, Hampton, VA 23681-2199 USA

An impedance prediction model was validated experimentally to determine the composite impedance of a series of high-aspect ratio slot resonators incorporating channel skew and sharp bends. Such structures are useful for packaging acoustic liners into constrained spaces for turbofan noise control applications. A formulation of the Zwikker-Kosten Transmission Line (ZKTL) model, incorporating the Richards correction for rectangular channels, is used to calculate the composite normalized impedance of a series of six multi-slot resonator arrays with constant channel length. Experimentally, acoustic data was acquired in the NASA Langley Normal Incidence Tube over the frequency range of 500 to 3500 Hz at 120 and 140 dB OASPL. Normalized impedance was educed using the Two-Microphone Method for the various combinations of channel skew and sharp 90^o and 180^o bends. Results show that the presence of skew and/or sharp bends does not significantly alter the impedance of a slot resonator as compared to a straight resonator of the same total channel length. ZKTL predicts the impedance of such resonators very well over the frequency range of interest. The model can be used to design arrays of slot resonators that can be packaged into complex geometries heretofore unsuitable for effective acoustic treatment.

I. Introduction

THE improved propulsion efficiency, afforded by the modern high-bypass turbofan engine and adopted by commercial aircraft in the 1960's, also allowed large reductions in jet mixing noise to be achieved. This fortunate circumstance was offset by increased tonal fan noise. During the initial decades of the turbofan era, fan noise was alleviated by a combination of passive liner treatments and nacelle modifications.[1,2] In their conventional form, passive liners consist of a honeycomb core bonded between a porous face sheet and an impervious backing plate. Such liners are treated as locally reacting in that individual honeycomb cells function as one-dimensional, tuned waveguides, independent of its neighbors. The acoustic absorption spectra of such structures are characterized by a single peak corresponding to the system resonance. As a result, this type of liner is bandwidth limited. One way to increase bandwidth is with cascaded layers judiciously tuned to different resonance frequencies, with the tradeoff increased cost, weight, and mechanical complexity.[3] Another approach (also not without design and fabrication complications) is to tune clusters of adjacent resonators to prescribed frequencies over bandwidths of interest.[4] The continuing push towards higher thrust ratings and lower thrust-specific fuel consumption implies increased by-pass ratios (BPR $\geq$ 6) with consequent greater fan diameters, fan chord lengths, and consequently, lower fan rotational speeds. This trend implies a continuing shift of the fan noise spectrum to lower frequencies, accompanied by a re-emergence of broadband noise as a contender with tonal noise in terms of community noise impact. Ultra-high bypass turbofans also imply engine nacelles that are shorter relative to their diameter thus limiting lined-duct-treatment-to-diameter ratio. This trend correlates inversely with liner effectiveness. Also, an increased engine nacelle diameter is generally not accompanied by a proportionate nacelle wall thickness increase to accommodate a deeper liner, which would ordinarily be required for conventional liner designs to mitigate lower frequency noise.

[1] Staff Engineer, Flight Systems Department, MS 463, Senior Member AIAA.
[2] Senior Research Scientist, Structural Acoustics Branch, MS 463.

Clearly, the more complicated liner designs, which have heretofore been considered cost prohibitive, are subject to reconsideration in more innovative strategies given new materials technology developments.

A. Packaging absorbing resonators in complex geometries

On a pure liner absorption efficiency basis, the engine design trends, suggested above, place an uncompromising limit on future increases in liner effectiveness, the efficacy of various nacelle and engine cycle modifications notwithstanding.[5] The motivation for the effort herein was to find new ways to leverage passive acoustic liner technology in portions of an engine heretofore unused. Practical applications hinge upon suitable packaging of conventional resonator absorbers into the space available while accommodating absorption bandwidth requirements, especially at the lower frequencies of interest.[6] The main obstacle to achieving low frequency performance is lack of liner depth. On a laboratory scale, it was previously demonstrated that the effective depth of a resonant absorber is predictably increased by skewing the resonator channel away from the usual orientation (normal to the local absorber surface)[7] as indicated in Fig. 1a. It is believed that further resonator packaging options can be implemented via an appropriate bend arrangement as suggested in the sketch of Fig. 1b. Clearly, if the acoustic effects of such bends are not detrimental, then the constraints on packaging resonant absorber arrays into any complex geometry are much less inhibitive than is the case for a single angle of skew as depicted in Fig. 1a. Thus it is of interest to assess the one-dimensional (1-D) waveguide propagation model for resonator channels subject to sharp bends as illustrated in Fig. 1b.

More specifically, it is the purpose of this paper to describe the results of an experiment to assess the applicability of 1-D acoustic propagation to high aspect ratio rectangular waveguides subjected to 90^o and 180^o bends. The goal is to predict the composite surface impedance of an array of unequal length resonator channels that might be configured similar to that shown in the sketch of Fig. 1b. The investigation is a continuation of the work described in Ref. 6 wherein resonator channel skew was achieved entirely by a single, oblique angle implemented at the resonator entry port. Results obtained in Ref. 6 demonstrated that the composite impedance of an array of skewed channels is reasonably predicted by a 1-D propagation model provided that the effective diameter of the high aspect ratio cross-section is properly quantified. In this investigation, multiple test model geometries sharing a common channel length and the same nominal hydraulic diameter are tested in the NASA Langley Normal Incidence Tube (NIT). Experimentally measured (educed) surface impedances are compared to predictions derived from the Zwikker-Kosten Transmission Line (ZKTL) model.[4]

II. Model Design, Experimental Setup, and Data Acquisition

Six test model configurations were fabricated for this investigation using a stereolithography process. Stereolithography allows the forming of solid, 3-D models from liquid plastic resin by application of laser light to harden the resin. A computer-controlled laser beam is scanned over the surface of the resin vat, tracing the area of one layer of a part causing that layer to harden. Successive layers are built up until the entire part is formed. Part tolerances are to within +/- 0.0635 mm (0.0025 in) of the target dimensions. To allow draining of excess liquid resin from within channels, the back plates were made detachable, each being secured with four bolts. A thin layer of petroleum jelly is used to seal the bottom plate.

The six plastic test model configurations are labeled C1-C6. All are embedded with an array of rectangular, cross-section channels, each with the same total length (inclusive of bends) of 171.5 mm (6.75 in). The channels are rigidly terminated, either by a back plate or within the structure itself and are intended to be acoustically isolated. They present an active area of 50.8 mm x 50.8 mm (2 in x 2 in) to the incident waves in the NIT as indicated by the superimposed square inset on the frontal view of a typical test model in Fig. 2. Side view photographs show the channel profiles of each configuration (C1-C6) in Figs. 3-9, respectively. Baseline configurations C1 and C2, shown in Fig. 4 and Fig. 5, respectively, consist of straight channels (normal to the active surface) and a skew of 45^o (implemented at the active surface). Figures 6-9 show configurations with 90^o and 180^o internal bends. Configurations C1-C5 have seven channels and C6 has 14 channels as shown in the plan view sketches of Fig. 10, along with the descriptive nomenclature. Detailed sketches of bend geometry are shown in Fig. 11.

The test model active surface precisely matches the active area of the NIT to provide an airtight seal for the test models. The composite impedance at the active surface is the parallel addition of the individual channel impedances with due regard for the open area ratio of ~20%. In addition to the same length, all channels have the same airway width of h=1.42 mm (0.056 in). Channel cross-section area is invariant (excluding bends) throughout the channel length – in contrast with those in Ref. 6 wherein cross-section area was skew angle dependent. The intent of the common channel length and cross section area invariance is to provide a direct experimental comparison of the anti-resonance responses for the different configurations. Configurations C1-C5 have the same lateral span of

S_1=50.8 mm (2 in). The sixth configuration, C6, has a span-wise partition of thickness, w_3=3.68 mm (0.145 in), to provide 14 channels with a lateral span of S_2=23.6 mm (0.929 in) and an aspect ratio of 16.6 (relative to an aspect ratio of 35.8 for the un-partitioned channels). The rationale for this split is given later. Five of the six configurations, C1 - C5, have different internal channel profiles implemented with 90° and 180° bends. The profile of C6 is the same as that of C5, the only difference being the mid-span partitioning described above. Open area ratios of the span-wise un-partitioned and partitioned channels are 19.6 and 18.1 %, respectively.

Impedance spectra for each sample were obtained in the NIT via the Two-Microphone Method (TMM).[8,9] A group of six electromagnetic acoustic drivers couple radially into a cylindrical tube that transitions to the 50.8 mm x 50.8 mm (2 in x 2 in) square cross-section waveguide. The key feature of the TMM is the efficient acquisition of the complex transfer function spectra between two, flush mounted microphones strategically located in the standing wave field from which the complex reflection factor is calculated. Transfer function accuracy is assured by a microphone switching technique that avoids labor intensive amplitude and phase calibrations. Figure 12 shows the general arrangement of the NIT apparatus. For all tests, acoustic excitation was random noise derived from a function generator whose output was low-pass filtered at 10 kHz. Data acquisition and analyses were performed from 500 to 3000 Hz with 25 Hz bin width. Data were acquired at overall sound pressure levels (OASPL) of 120 dB and 140 dB determined by integrating from 500 to 3000 Hz as measured by a third, calibrated, reference microphone located a fraction of the shortest wavelength of interest from the sample face. A computer controlled spectrum analyzer was employed in conjunction with custom software to acquire acoustic data and generate output files for analysis. A test model clamped into place via a specially machined holding fixture affixed to the NIT is shown for C3 in Fig. 13.

III. Waveguide Propagation Model

A. Limits on 1-D propagation theory through sharp bends in rectangular waveguides

As mentioned previously, the 1-D impedance prediction model has been validated for skew angles of up to 60° implemented at the test model active surface.[7] In the present investigation, we wish to extend that validation to include internal channel bends of 90° and 180°. This possibility would allow greater design latitude for highly constrained spaces within a turbofan engine. From the literature, it is known that such sharp bends can exhibit significant transmission losses (thus affecting impedance looking into the bend), depending upon the non-dimensional frequency parameter, *kh*, where *k* is the free-space wave number and *h* is a characteristic width of the waveguide. Previous work was motivated mainly by concerns with transmission losses through sharp bends in HVAC ducting and reactive type silencers for internal combustion engines where *kh* values are relatively high (≥ 0.5).[10,11,12,13] For low *kh* values (≤ 0.1), as is the case for the present application, 1-D propagation is expected to hold, with sufficient accuracy, through such bends. A complication arises, however, in that for some potential applications, it may be desirable to make the duct width, h, sufficiently small such that the visco-thermal losses contribute a modest acoustic resistance. This occurs when h is such that the acoustic boundary layer occupies a significant portion of the channel cross-section. Fortunately, small *kh* values also help to assure the applicability of 1-D propagation through channel bends. A potential issue is that at high acoustic particle velocities, laminar flow separation at the bend corners may add a substantial nonlinear resistance. Of course, rounded bends can, in theory, eliminate such laminar flow separation, but likely with more complicated design and packaging. The present investigation aims to experimentally assess the ZKTL propagation model for high aspect ratio, terminated, rectangular waveguides (i. e. resonator channels) with intervening sharp bends where the channel width, *h*, is such that visco-thermal losses due to the acoustic boundary layer thickness generate a small, but measurable resistance. For arrays of channels with different lengths, the anti-resonance resistance peak is subdued and parallel addition of channel impedances yields a stable, composite impedance with anti-resonance peaks in resistance dramatically reduced – if not eliminated. This circumstance raises the possibility for packaging such configurations, as per Fig. 1b, to attain extended absorption bandwidth in highly restricted and irregular spaces. Extended bandwidth in such composite systems subsumes one or more channel anti-resonance impedance peaks that tend to perturb the desired impedance spectrum. Thus channel width becomes an important design parameter for attaining extended absorption bandwidth.

B. The Zwikker-Kosten waveguide propagation model

Experimental results are compared to impedance model predictions via the NASA-Langley Zwikker-Kosten Transmission Line (ZKTL) waveguide propagation code. This code is based upon an approximate, analytical solution for the propagation constant, Γ, in a straight, cylindrical tube as given by Zwikker and Kosten[14] in 1949.

The full, exact solution for Γ, as derived by Kirchoff in 1868, involves complex transcendental functions and must be solved numerically. This was first accomplished by Tijdeman[15] in 1975 by formulating the transcendental equation in the form:

$$F(\Gamma, s, \bar{k}, \sigma, \gamma) = 0 \tag{1}$$

where s is the shear wave number

$$s = a\sqrt{\rho\omega / \mu} \tag{2}$$

and a is the tube radius, $\bar{k}$ is the reduced frequency,

$$\bar{k} = \omega h / c (= kh) \tag{3}$$

and σ is the square root of the Prandtl number (ratio of viscous diffusion rate to thermal diffusion rate),

$$\sigma = \sqrt{\mu C_p / \kappa} \tag{4}$$

and γ is the ratio of specific heats where C_p and C_v are the heat capacity of gas at constant pressure and volume respectively.

$$\gamma = C_p / C_v \tag{5}$$

Numerous approximate solutions documented in the literature (denoted by adjectival descriptors like "narrow" and "wide" tube) are reviewed and critiqued by Tijdemann. In this critique, he concluded that the so-called low-reduced-frequency solution by Zwikker and Kosten covered, with good accuracy, the entire range of the narrow-to-wide tube approximate solutions reported in the literature, provided that both the reduced frequency and shear wave numbers comply with the restrictions, $\bar{k} << 1$ and $\bar{k} / s << 1$. It is of interest to review the physical implications of these restrictions as stated in Ref. 14:

1) The medium is homogeneous which means that the wavelength and tube radius must be large compared to the molecular mean free path (i.e. frequency is restricted to be < 100 MHz and tube radius must be > 100 microns);
2) No steady flow;
3) Small amplitude, sinusoidal perturbations (no circulation and no turbulence);
4) The tube is long enough, so that end effects are negligible.

The following boundary conditions also apply:

1) The tube wall is rigid;
2) Radial fluid velocity is zero on the tube axis and all acoustic field variables must remain finite there;
3) Thermal conductivity and capacity of the wall is large compared to that of the propagating medium, i.e. wall is isothermal.

Given the above assumptions and restrictions, the Zwikker-Kosten propagation constant, Γ, for a cylindrical tube is given by:

$$\Gamma = \sqrt{\frac{J_0(i^{3/2}s)}{J_2(i^{3/2}s)}}\sqrt{\frac{\gamma}{n}} \tag{6}$$

where J_n is the n-th order complex Bessel function and n is a complex polytropic constant that specifies the nature of the thermodynamic process for the sound propagating medium in the tube (air).

$$n = \left[1 + \frac{\gamma - 1}{\gamma} \frac{J_2(i^{3/2}\sigma s)}{J_0(i^{3/2}\sigma s)} \right]^{-1} \tag{7}$$

Note that the parameter group, σs, is independent of viscosity, which means that n is related only to heat conduction from the air into the tube wall. As $\sigma s \rightarrow 0$, the process approaches isothermal, (i.e. $n \rightarrow 1$) and as σs becomes large, $n \rightarrow \gamma$, (i.e. the process approaches adiabatic). If the assumption of a perfectly conducting tube wall is deemed unacceptable, then the idealization implied by Eq. (7) does not apply. For air and the common materials likely to be encountered in this application, the idealization is reasonable. The tube characteristic impedance (dimensionless) is given by:

$$\zeta_c = \frac{-i}{\Gamma} \frac{J_0(i^{3/2}\sigma s)}{J_2(i^{3/2}\sigma s)} \tag{8}$$

Equations (6-8) are the core ingredients of the ZKTL transmission line code. To see how these relate to the physics of propagation in a tube with visco-thermal dissipation at the tube walls, it is of interest to consider the Kirchoff approximation to the Zwikker-Kosten solution given by Eq. (6) for Γ as follows.

$$\Gamma = \left\{ \frac{1}{\sqrt{2}} \left(\frac{\gamma - 1 + \sigma}{\sigma s} \right) + i \left(1 + \frac{1}{\sqrt{2}} \left(\frac{\gamma - 1 + \sigma}{\sigma s} \right) \right) \right\} \tag{9}$$

In this approximation, the real and imaginary parts of Γ are split as per $\Gamma = \Gamma' + i\Gamma''$ where the real part relates to the attenuation rate and the imaginary part relates to the spatial phase rate. In dimensional units, the spatial variation in the positive going pressure wave (+$i\omega$t convention) is given by:

$$p \approx e^{-k\Gamma x} = e^{-k(\Gamma' + i\Gamma'')x} = e^{-k\Gamma' x} e^{-ik\Gamma'' x} \tag{10}$$

The terms $e^{-k\Gamma' x}$ and $e^{-ik\Gamma'' x}$ represents exponential decay and spatial phase rate of the pressure along the tube in nepers and radians per unit distance, respectively. A cursory examination of Eq. (9) reveals that in the limit as σs increases without bound (accomplished by decreasing viscosity, increasing diameter, increasing frequency, increasing tube diameter, or any combination of these), the attenuation approaches zero and the phase rate corresponds to the adiabatic sound speed, consistent with propagation in the absence of visco-thermal effects. Also, from Eq. (3), it can be shown that the characteristic impedance approaches unity in the limit of large σs, i.e. when visco-thermal effects become negligible. It is clear that the dimensionless parameter, σs, completely accounts for visco-thermal effects on sound propagation in tubes under the restrictions and assumptions stated. The adjectival descriptors "narrow-tube " and "wide-tube" found in the literature, arise from the observation that the tube velocity profile goes from very nearly parabolic (for "small" values of σs) to very nearly flat (for "large" values of σs). Thus these descriptions are somewhat misleading in that "narrow" and "wide" tube behavior is ultimately determined by the parameter, σs.

C. The Richards correction for rectangular cross section

To calculate the propagation constant of a tube with rectangular cross-section, we adopt the artifice proposed by Richards[16] wherein an equivalent cylindrical tube radius is equated to a generalized radius, *g*, as calculated from

$$g = 2\left(\frac{S}{P} \right) \tag{11}$$

where *S* is the channel area and *P* is the channel perimeter. This equivalency was proposed by Richards based on comparing an exact solution for propagation between infinite parallel plates with the Zwikker-Kosten solution for propagation in a cylindrical tube. For a circular cross-section, the geometric radius, *R*, and generalized radius, *g*, are

equal, and in the limit of infinite, parallel plates separated by width h, g=h, (i.e. $\underset{s\to\infty}{Lim}\langle g\rangle = h$). For an infinite parallel, flat plate separation of h=10 mm and cylindrical tube of radius R=10 mm, Richards found that the propagation constants, when using the generalized radius, were essentially identical (within graphical resolution of Ref. 16) over the frequency range, 100 to 5000 Hz. When the tube radius and plate separation were reduced to 0.6 mm, the two propagation constants exhibited a small systematic error on the graphical resolution employed, but the overall accuracy was still good. At a plate separation of 0.1 mm and tube radius of 0.1 mm, a very significant difference between the two propagation constants was evident. The Richards results suggest that for the high aspect ratio channels, such as employed here (i.e. greater than about 10) and airspace widths greater than about 0.5 mm, use of the generalized radius, g, in the Zwikker-Kosten propagation model is acceptable.

D. The ZKTL impedance prediction code

The normal incidence impedance of an array of parallel channels is calculated by parallel addition of the individual channel impedances. Individual channel impedances are calculated from the Zwikker-Kosten transmission line model described previously. No interaction effects between channels are included in this model. This means that the relative locations of channels play no role in the composite impedance if the array can be considered acoustically compact, i.e. trace wavelength on the active surface is about 10 times the array characteristic dimension. In the present case the highest frequency for which this criterion is satisfied is about 700 Hz (grazing incidence). At near normal incidence this issue goes away, because the trace wavelength for even the highest frequency approaches infinity. This is an important assumption in that it removes any constraint on the relative positioning of resonator ports to achieve a desired composite impedance. This is potentially of great utility in the packaging issue for irregularly shaped volumes.

The ZKTL impedance prediction code uses a transfer function format to calculate the impedance of an individual channel, consisting of multiple elements, as indicated in Fig. 14 which shows the labeling scheme used to define such a multi-element channel. Wave transmission through a dissipative channel can be described by a forward transmission matrix of the following form:

$$\begin{pmatrix} p(x_{n+1}) \\ u(x_{n+1}) \end{pmatrix} = \begin{pmatrix} T_{11} & T_{12} \\ T_{21} & T_{22} \end{pmatrix} \begin{pmatrix} p(x_n) \\ u(x_n) \end{pmatrix}, \tag{12}$$

Where T_{11}=T_{22}=cosh($k\Gamma L$), T_{12}=$\zeta_c$cosh($k\Gamma L$), and T_{21}=ζ_c^{-1}cosh($k\Gamma L$) with Γ as the propagation constant, ζ_c as the characteristic impedance, k as the free-space wave number and L as the channel depth. The terminating condition for each channel was assumed to be a rigid, impervious boundary expressed in matrix form as:

$$\begin{pmatrix} p(x_0) \\ u(x_0) \end{pmatrix} = \begin{pmatrix} 1 \\ 0 \end{pmatrix} \tag{13}$$

A more detailed discussion of the prediction model and its application to the current geometries can be found in Ref. 4. Should it be necessary to include bend effects explicitly, the transfer matrix format above can easily be extended to include either a theoretical or experimental bend transfer matrix as per the work of Lippert.[11,12] It is one goal of the present investigation to assess the need for such bend transfer functions.

E. The Cummings model for inviscid propagation through a 180^o bend

It is important to recognize that at sufficiently high kh values, an incremental mass reactance is expected from inviscid propagation through a sharp bend (apart from any distributed visco-thermal resistance and nonlinear resistance concentrated at the bend, alluded to earlier). Physically, this reactance increment is associated with the additional momentum necessary to turn the wave motion around the bend. This effect would be included under a more complete model analysis involving higher order modes in the channel bend as was done by Cummings[13] for inviscid wave propagation, since his main concern was with HVAC and expansion chamber mufflers. At the geometric scale of interest here, a modal approach that includes visco-thermal effects is beyond the scope of this effort. Instead, we use the Cummings first order solution result to estimate bend effects on inviscid propagation through a 180^o bend, at the kh values of interest for the present application, and compare with the Zwikker-Kosten, 1-D model that includes visco-thermal effects.

For completeness, the Cummings first order solution for the reflection factor, *r*, of a rigidly terminated channel including a 180° bend is repeated here as given by Eq. (25, 26) of Ref. 13 with minor notational changes:

$$r = Exp[-i2kb]*$$
$$\left\{\frac{\left(2\cot(k_{x3}^1 b)+\frac{k_{x3}^1}{k}\cot(kL)+\frac{\cot(kL)}{\cot(kb)}\cot(k_{x3}^1 b)\right)+ i\left(2\frac{k_{x3}^1}{k}\frac{\cot(kL)}{\cot(kb)}\cot(k_{x3}^1 b)+\frac{\cot(k_{x3}^1 b)}{\cot(kb)}+\frac{k_{x3}^1}{k}\right)}{\left(2\cot(k_{x3}^1 b)+\frac{k_{x3}^1}{k}\cot(kL)+\frac{\cot(kL)}{\cot(kb)}\cot(k_{x3}^1 b)\right)- i\left(2\frac{k_{x3}^1}{k}\frac{\cot(kL)}{\cot(kb)}\cot(k_{x3}^1 b)+\frac{\cot(k_{x3}^1 b)}{\cot(kb)}+\frac{k_{x3}^1}{k}\right)}\right\} \tag{14}$$

where *b* is the bend depth in the x-direction (see Fig. 11) and

$$k_{x3}^1 = \sqrt{k^2-\left(\frac{\pi}{2h}\right)^2} \tag{15}$$

where *k* is the free-space wave number and *h* is the channel width. The coordinate system for the Cummings model is overlaid on the 180° bend geometry depicted in Fig. 11. Note that the channel partition thickness of *w3* is taken as zero in the Cummings model. This constitutes the main shortcoming of this model for estimating bend inertial effects in the present context. The channel width, *h*, is seen to enter only through Eq. (15) for calculating k^1_{x3}.

IV. Discussion of Results

A. Inviscid bend effect via Cummings model relative to the 1-D impedance model

To lend insight into the forthcoming comparisons of the measured and predicted impedance spectra via the Zwikker-Kosten model, it is of interest to compare the channel reactance as calculated using the conventional, 1-D impedance model, –cot[kL], and the first order model due to Cummings that accounts for a 180° bend. An inviscid fluid is assumed for both models to give a zero resistance. For convenience, the calculations are done for a single channel since no experimental results are involved. The rigidly terminated channel is set to a length of 171.5 mm (designed to give resonance/anti-resonance frequency sequence at 0.5 kHz increments, starting at 0.5 kHz) and the airway width is set to 1.42 mm. Figure 15 shows the comparison. The blue and red curves correspond to the -cot[kL] and Cummings models, respectively. The momentum turning associated with the bend displaces all resonance/anti-resonances very slightly downward. These small displacements increase with frequency. At 3.0 kHz, this frequency displacement, for the anti-resonance frequency, is estimated to be not more than about 25 Hz. This small effect can evidently be dismissed for the present application for the current frequency range of interest.

B. Comparison of measured and predicted impedance spectra

Figures 16-22 show comparisons of measured and predicted impedance spectra (ZKTL model) for the six test configurations. Normalized resistance and reactance are obtained from 0.5 kHz to 3.5 kHz in 25 Hz intervals for an incident OASPL on the active surface of 120 dB. In all the graphics, the red and blue solid curves represent predicted resistance and reactance, respectively and red and blue symbols represent the measured resistance and reactance, respectively.

Figure 17 shows the results for test configuration C1 (baseline straight channels of depth 171.5 mm). Over the frequency range (500 to 3500 Hz), four resonances are observed at 1 kHz intervals (zero reactance crossings) starting at approximately 0.5 kHz and ending at 3.5 kHz. Likewise, three anti-resonances are observed at 1 kHz intervals, starting at 1 kHz. It should be noted that graphical resolution of the anti-resonances is much better than the resonances because of the steeper slope at the zero crossings. The measured reactance resonance and anti-resonance

zero crossings exhibit small, but discernable, downward frequency displacements relative to the predicted results. This is caused by sound speed reduction associated with visco-thermal dissipation. There is no bend-induced momentum turning in this baseline configuration. This result is consistent with the design intent for this test configuration. Measured and predicted impedances are in excellent agreement up to about 3.4 kHz in spite of the possibility of higher order modes that tend to cut on in the vicinity of 3.3 kHz.

When an angle of 45^o is introduced at the active surface of configuration C2 (Fig. 18), the measured data are nearly identical to that from C1 apart from a slight divergence between data and model between at 3.0 to 3.3 kHz. The 45^o skew angle for C1 and associated increased in open area ratio at the test model face seem to have little effect on the measured impedance. On-the-whole, the model results compare well with measurement up to 3 kHz with a slight over-prediction of the reactance at 3 kHz to about 3.3 kHz. Data from configurations C3 and C4 with single and multiple 90^o bends (Figs. 19, 20) continue this behavior. It was speculated pre-test that the impedance of each segment (between bends) might exhibit ¼ wavelength resonance, but no evidence of this was discerned. The results lead to a conclusion that overall channel length is the prime factor controlling characteristic impedance.

Configuration C5 produced measured results that differed significantly from the predicted values with large shifts in the magnitude and frequency of the reactance crossover points and peaks (Fig. 21). Given the compact geometry of the channel packaging resulting in relatively thin channel walls, it is likely that there was insufficient acoustic isolation between these channels. Such crosstalk was not modeled by the ZKTL code possibly leading to the observed differences. Configuration C6 was constructed with a septum that divided the seven channels into 14 in an attempt to stiffen the channel walls to increase isolation. Better agreement can be seen between the impedance measurements and analytical results for this configuration although the third anti-resonance peak exhibits a slight shift downward in frequency (Fig. 22). These results suggest that channel-to-channel isolation must be maintained for predictable acoustic performance.

Measurements were repeated for all configurations with the sound pressure level increased to 140 dB OASPL to determine if any nonlinearity effects were present. Results matched the 120 dB values across the frequency range and are thus omitted for the sake of brevity.

C. Packaging issues to attain improved bandwidth at low frequencies

The generally excellent ability of the ZKTL model to predict the composite surface impedance of an array of high aspect ratio, rectangular channels with sharp bends (including skew introduced at the active surface), suggests a wide range of options for packaging such resonant systems into irregular and depth limited spaces for turbofan applications. It is beyond the scope of this paper to suggest real-world applications with any degree of specificity. However, it of interest to highlight the salient attraction of employing such resonant systems, on the scale discussed above, to achieve increased bandwidth, especially at lower frequencies, with severe liner volume constraints. To that end, Fig. 23 shows a linear stepped array of 21 parallel channel resonators (presumed to be within the *kh* range discussed above). The minimum and maximum channel lengths are about 3 and 30 mm, respectively. By paring these channels (longer-to-shorter) sequentially, it is evident that 180^o bends can be employed to reduce the maximum length to about 15 mm. The composite reactance for this array, obtained by parallel addition, is shown in Fig. 24 as red curves (solid for resistance; dashed for reactance). For comparison, the reactance is also shown for the 21 channels set to a constant depth of 30 mm as the green curves (solid for resistance; dashed for reactance). The sole motivation of this approach is to drive the reactance curve closer to zero which is surely demonstrated by this very generic example. Note that resistance is small, but not zero, on this scale. (In an actual application, resistance could be supplemented with the addition of a face sheet.) In terms of bandwidth improvement, if we assume that the reactance of the mult-depth array at 0.5 kHz is acceptable at about -1.5 $\rho\chi$, then the bandwidth of the single depth array is not more than about 1 kHz, centered on about 2.7 kHz. Thus the multi-depth array has achieved a bandwidth improvement by a factor of at least three, relative to the single-depth array.

V. Conclusion

Experiments were conducted to determine the impedance spectra for a series of seven rectangular channels, rigidly terminated at a length of 171.5 mm and with the high aspect ratio cross-sections of about 16 and 36 with a small dimension of 1.42 mm. Channel skew, with respect to the active surface, and 90^o and 180^o bends were introduced to investigate the ability of the 1-D, Zwikker-Kosten model to predict the impedance of the various test configurations. Measured and predicted impedance values were found to be in excellent agreement for all configurations with the exception of the configuration using 180^o bends for the highest aspect ratio case in which case coupling between adjacent channels was present. The discrepancy between experiment and model prediction is attributed to channel partition vibration. Excellent agreement between experiment and model prediction was restored

by adding a span-wise partition to decrease the aspect ratio (increased partition stiffness) by about 50%. No nonlinear behavior was observed for band-limited, random excitations of 120 dB and 140 dB OASPL.

These results validate the usage of the ZKTL impedance prediction model for high-aspect ratio rectangular channels provided that the Richards generalized radius is employed in the ZKTL model. This generalized radius is restricted to values above about 0.5 mm.

Assuming the ZKTL model to hold for parallel addition of multiple channel arrays with different channel lengths, it is shown analytically that the reactance values can be driven significantly toward zero over a frequency range from 0.5 to 3.5 kHz, relative to that for a single depth array, thus increasing absorption bandwidth significantly. This result remains to be verified experimentally for the range of restricted *kh* values of interest in the application of multiple depth resonator arrays to turbofan noise reduction applications. Once verified, ZKTL may be applied in the development of innovative packaging solutions for complex liner geometries.

Acknowledgments

The authors would like to thank Michael G. Jones and Carol C. Harrison of NASA Langley for his assistance in preparing some of the figures used in this paper and her efforts to acquire the impedance data shown herein.

References

[1]"The NASA acoustically treated nacelle program," *Proceedings of the Aircraft Noise Symposium* (Acoustical Duct Treatments for Aircraft), Invited Tutorial Papers presented at the 77th Meeting of the Acoustical Society of America, 8, Apr. 1969, Philadelphia, PA.

[2]"Study and Development of Turbofan Nacelle Modifications to Minimize Fan-Compressor Noise Radiation," Volume IV – Flight-worthy Nacelle Development, Prepared by The Boeing Company, NASA CR-1714, Jan. 1971.

[3]Bielak, G. W. Premo, J. W., and Hersh, A. S., "Advanced Turbofan Duct Liner Concepts," *NASA CR-1999-209002*, 1999.

[4]Parrott, T.L., Jones, M. G., "Parallel-element liner impedances for improved absorption of broadband sound in ducts," *Noise Control Engineering Journal*, Vol. 43, No. 6, Nov. 1995.

[5]Huff, Dennis L., "Noise Reduction Technologies for Turbofan Engines," NASA TM 2008-214495, September 2007.

[6]U. S. Patent: Low Noise Fan Exit Guide Vane, 7,334,998.

[7]Parrott, T.L., Jones, M. G., Homeijer, B., "Effect of Resonator Axis Skew on Normal Incidence Impedance," AIAA 2003-3307, Jul. 2003.

[8]"Standard Test Method for Impedance and Absorption of Acoustical Materials using a Tube, Two Microphones, and a Digital Frequency Analysis System," ASTM E1050-90, 1990.

[9]Jones, M. G., and Stiede, P. E., "Comparison of Methods for Determining Specific Acoustic Impedance," *Journal of the Acoustical Society of America*, Vol. 101, No. 5, 1997, pp. 2694−2704.

[10]Lippert, W. K. R., "A method of measuring discontinuity effects in ducts," *Acoustica*, Vol. 4, No. 2, 1954, pp 307-312.

[11]Lippert, W. K. R., "The measurement of sound reflection and transmission at right angle bends in rectangular tubes," Acoustica, Vol. 4, No. 2, 1954, pp 313-319.

[12]Lippert, W. K. R., "Wave transmission around bends of different angles in rectangular ducts," *Acoustica*, Vol. 5, 1955, pp 274-278.

[13]Cummings, A., "Sound transmission in 180^o bends of rectangular section," *Journal of Sound and Vibration,*Vol. 41, No. 3, 1975, pp. 321-334.

[14]Zwikker, C. Kosten, C., "Sound Absorbing Materials," Elsevier, Amsterdam, 1949.

[15]Tijdeman, H., "On the Propagation of Sound Waves in Cylindrical Tubes," *Journal of Sound and Vibration*, Vol. 39, No. 1, 1975, pp 1-33.

[16]Richards, W. Bruce, "Propagation of Sound Waves in Tubes of Noncircular Cross Section," NASA TP 2601, Aug. 1985.

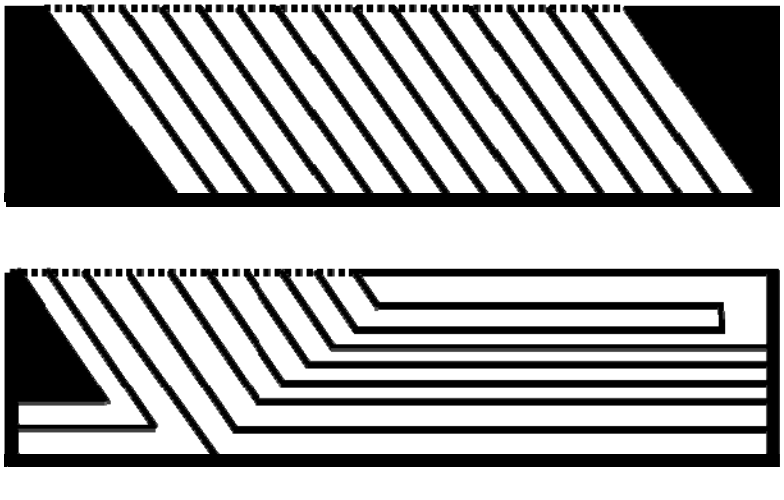

Figure 1. Example liner configurations: (a) Skewed resonators packaged as a conventional liner. (b) Resonators combining skew and bends to increase resonator length and maximize available space.

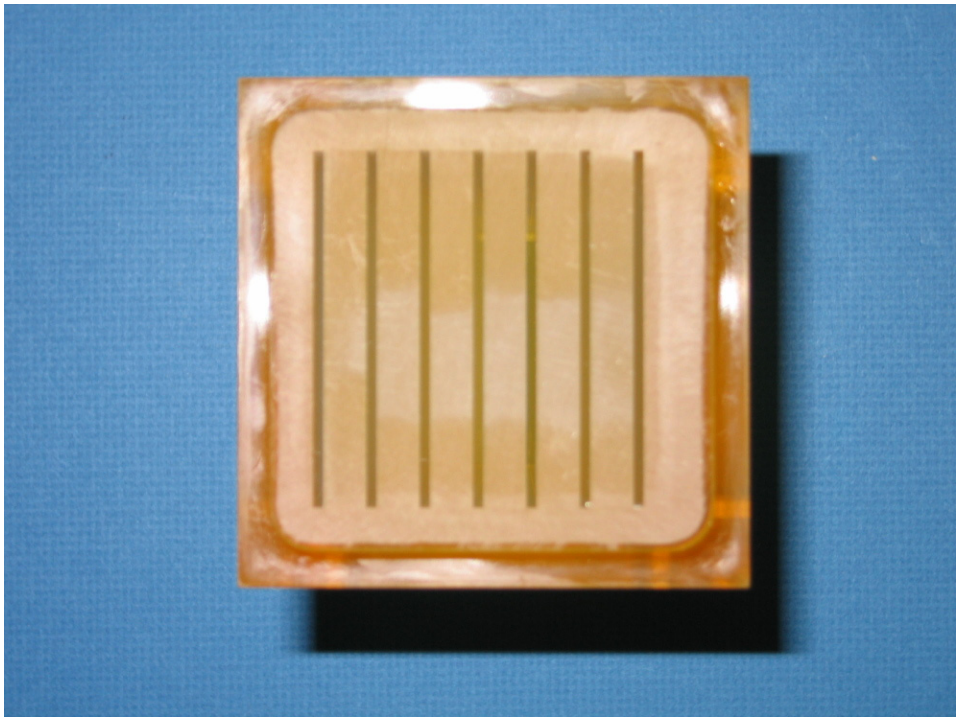

Figure 2. Typical test model face showing uniform spacing of seven high aspect ratio slot resonators.

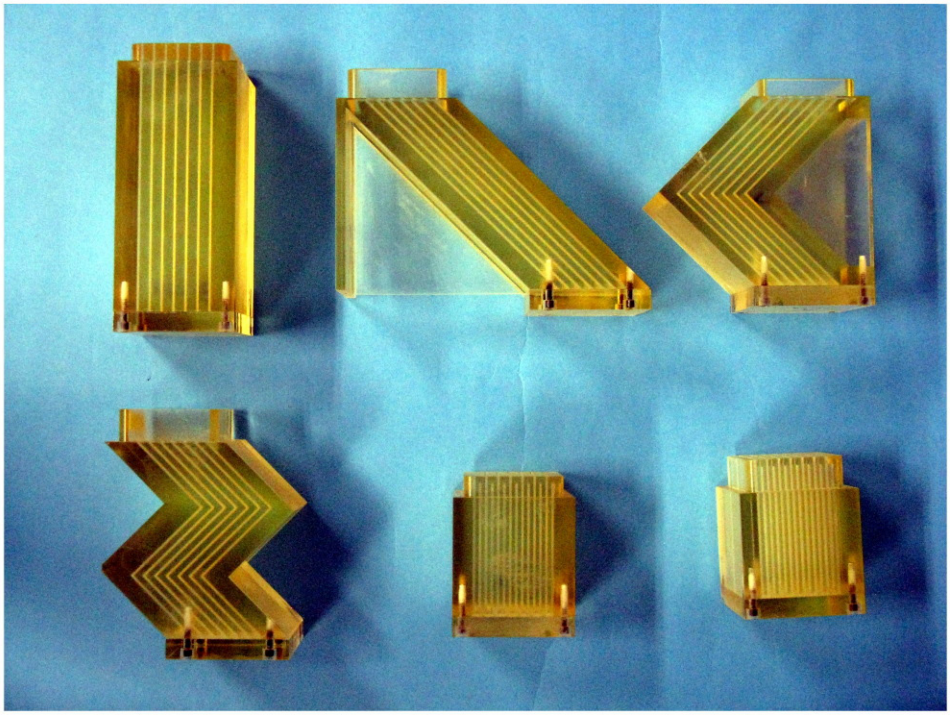

Figure 3. Test model configuration profiles - reading from left-to-right and down: C1 - baseline straight, C2 - 45^{o} skew, C3 - single 90^{o} bend, C4 - double 90^{o} bend, C5 - 180^{o} bend – no span-wise partitioning, C6 - 180^{o} bend with lateral partitioning

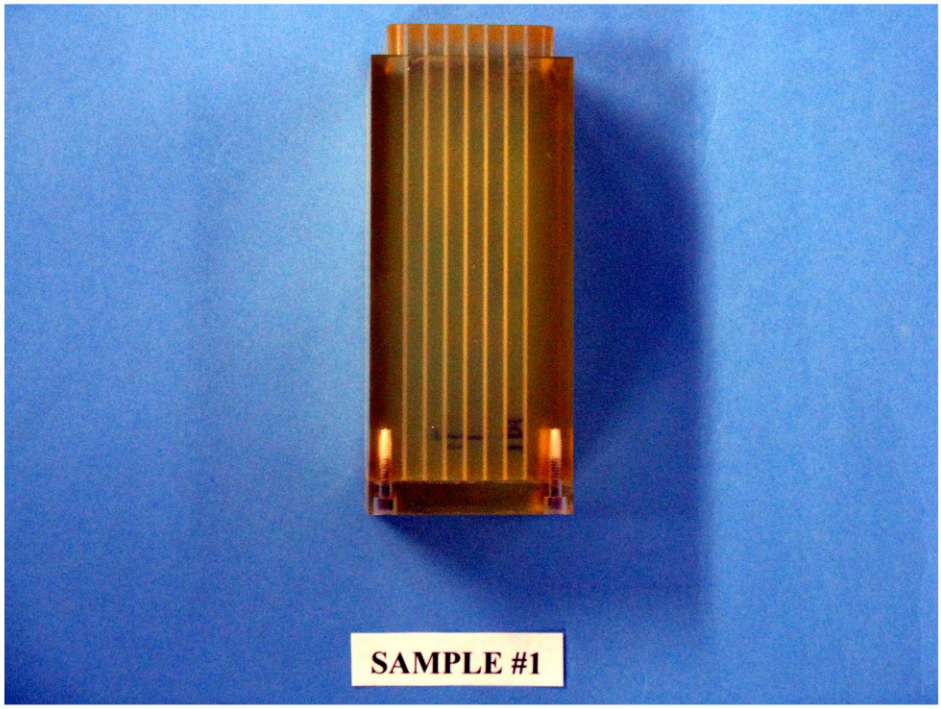

Figure 4. Configuration-C1 (baseline - straight channels).

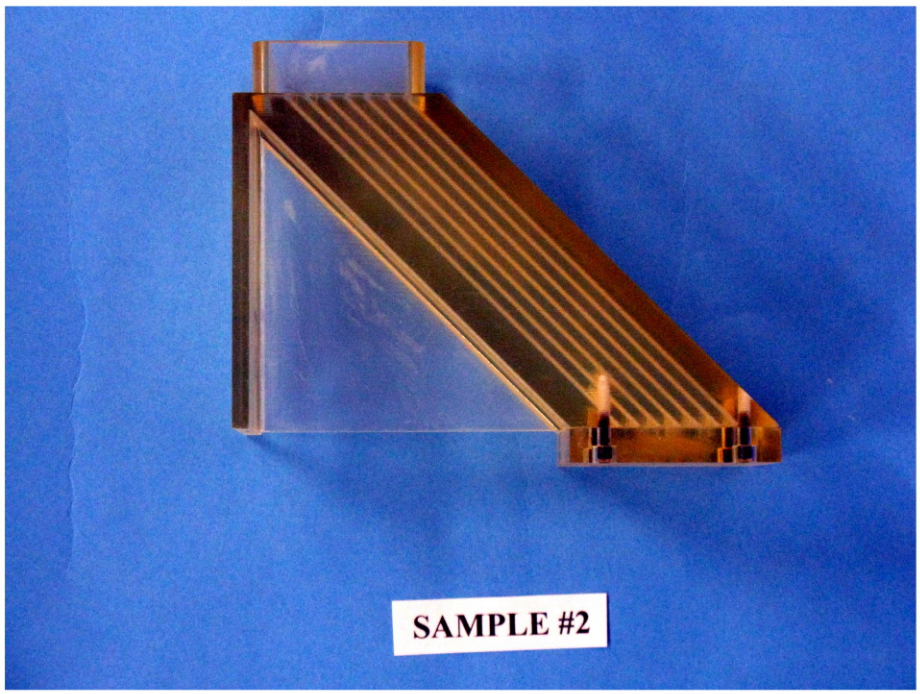

Figure 5. Configuration-C2 (45^{o} skew).

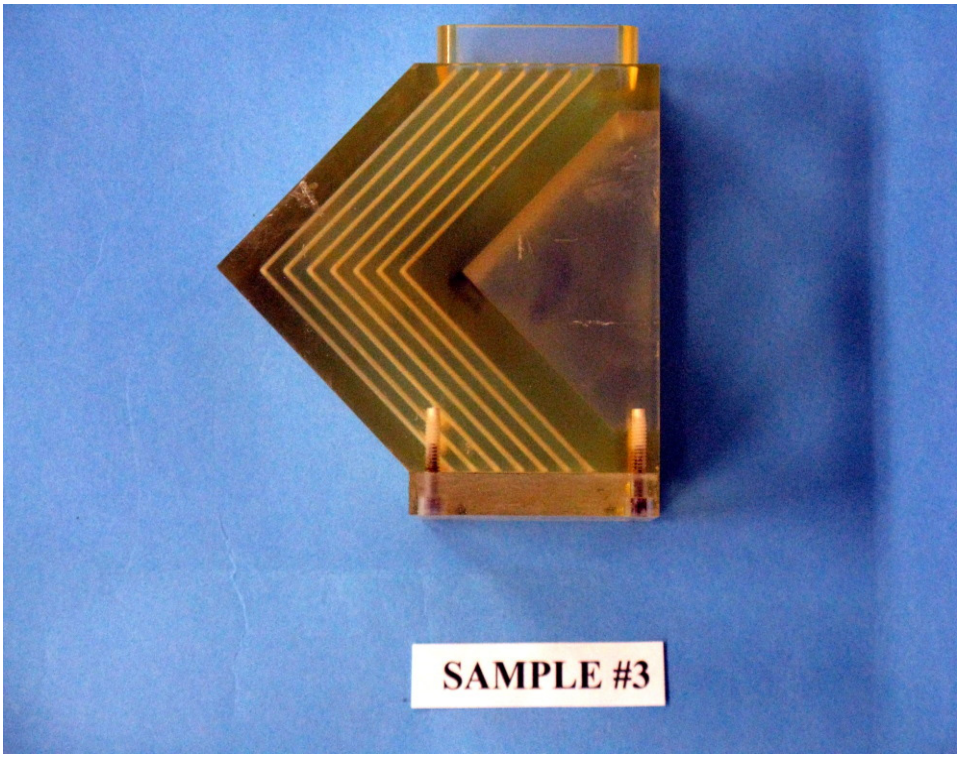

Figure 6. Configuration-C3 (single 90^{o} bend).

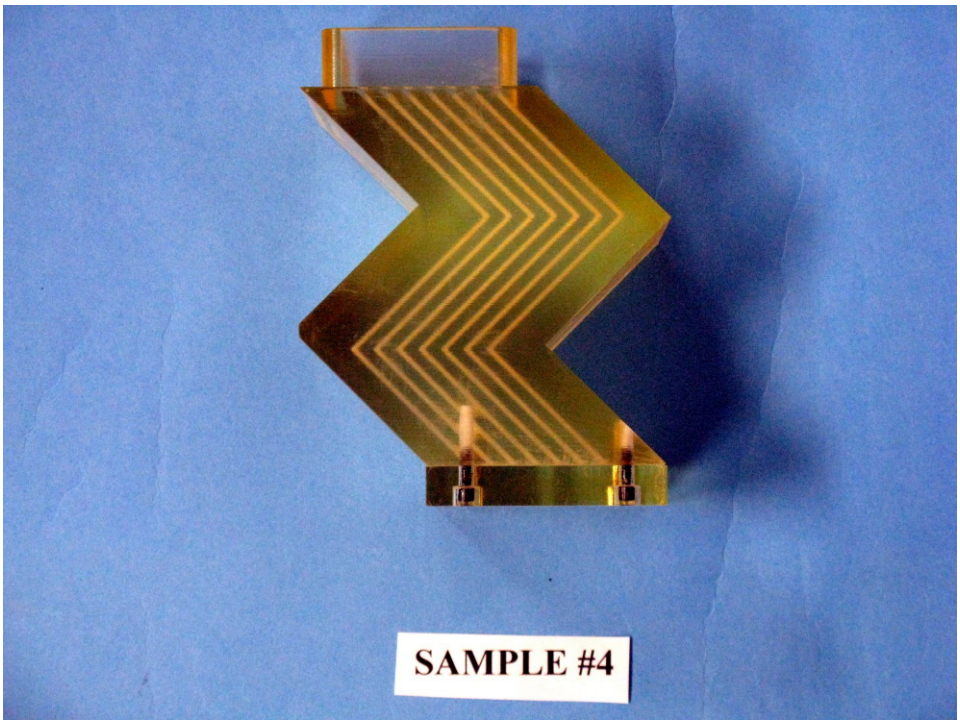

Figure 7. Configuration-C4 (two 90^{o} bends).

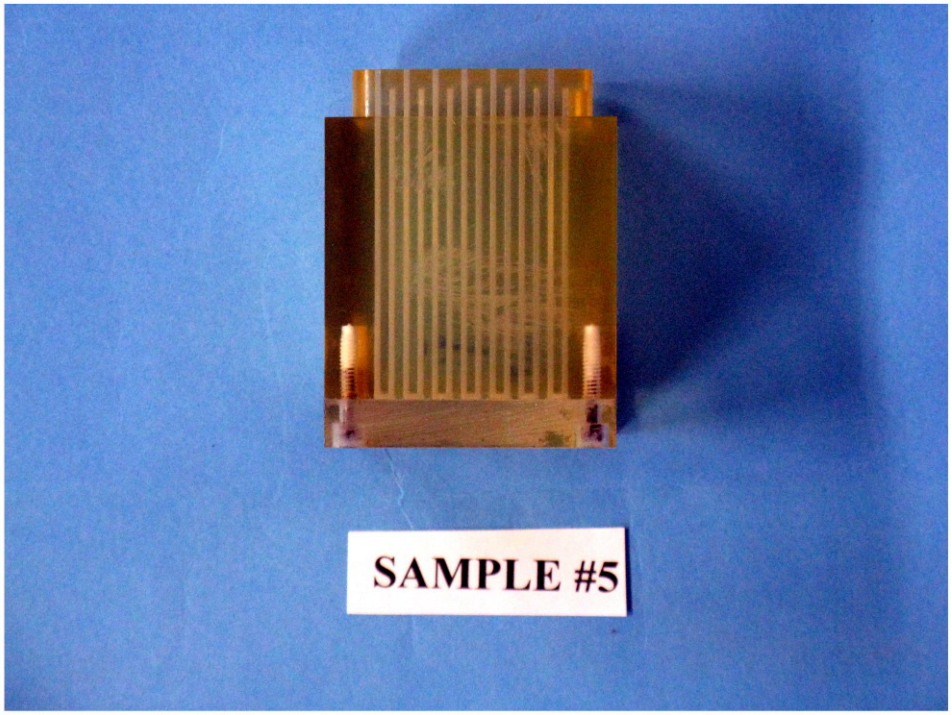

Figure 8. Configuration-C5 (180^{o} bend with no span-wise partitioning).

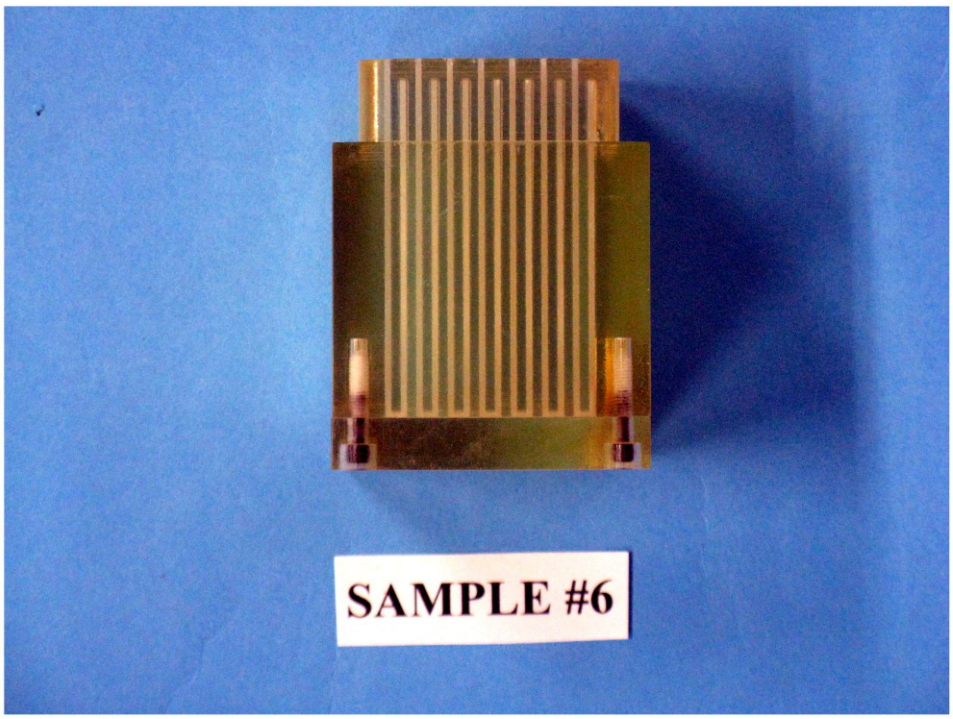

Figure 9. Configuration-C6 (180^{o} bend with span-wise partitioning).

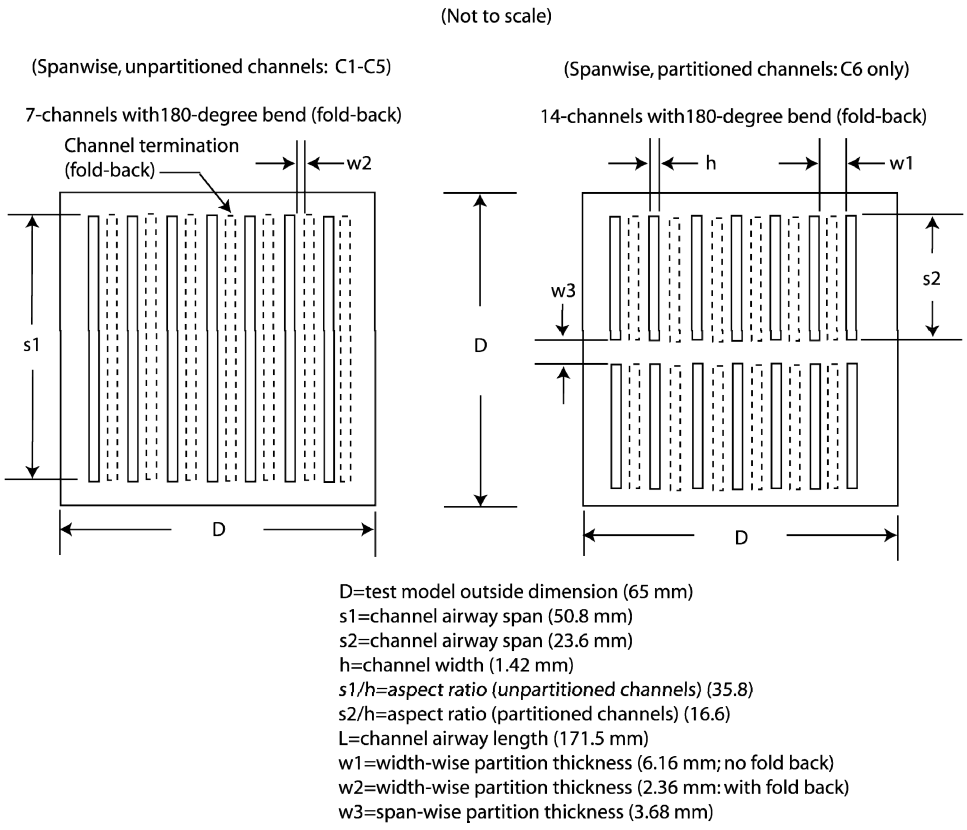

Figure 10. Typical view of test model active surface with relevant nomenclature.

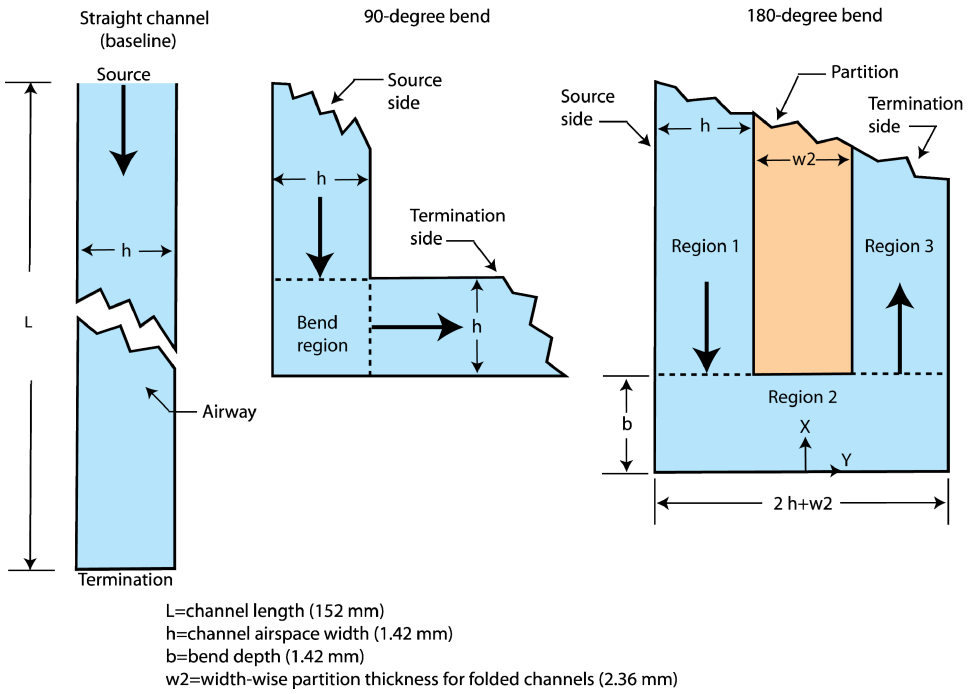

Figure 11. Typical Detail of 90° and 180° bend geometry with relevant nomenclature.

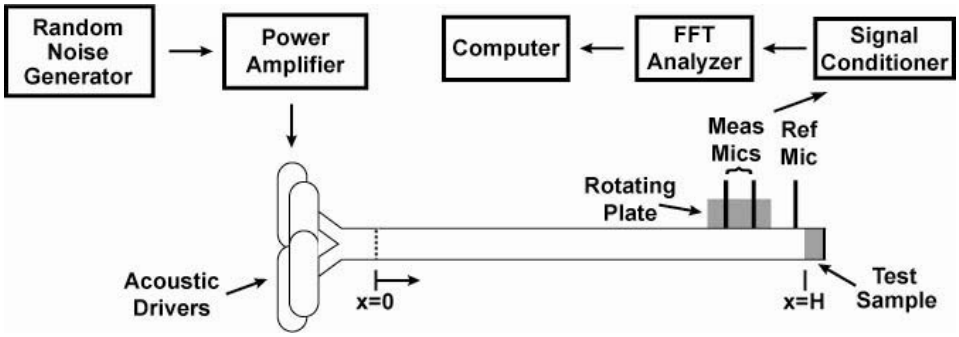

Figure 12. NIT general arrangement.

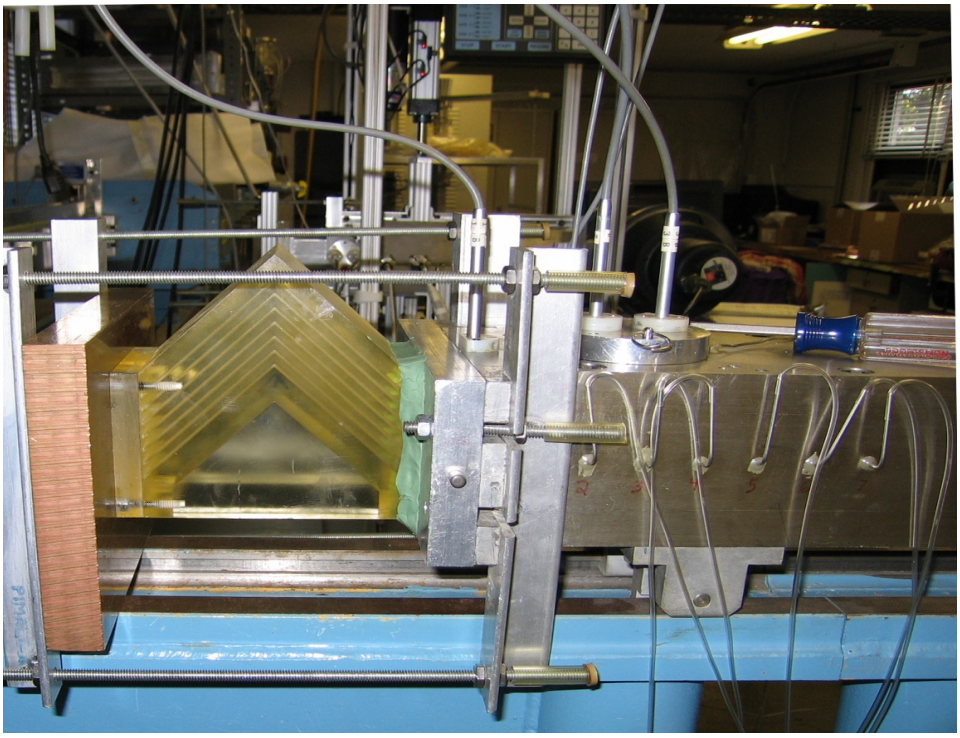

Figure 13. Configuration-C3 installed in the NIT via position fixture and clamping arrangement.

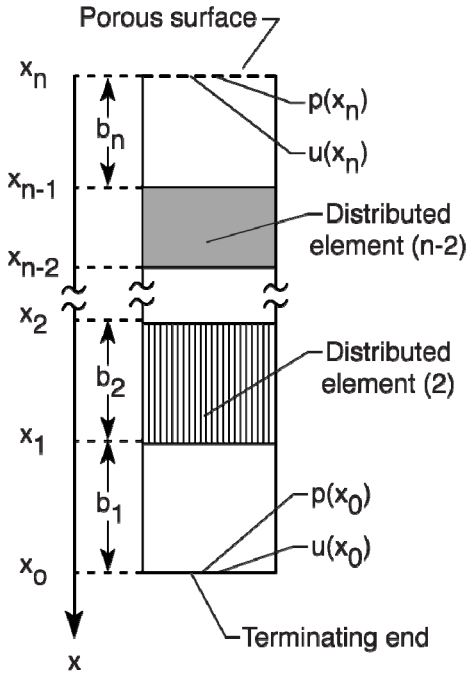

Figure 14. Labeling scheme for elements in a single, isolated channel of a multi-channel resonator system that is amenable for the 1-D Zwikker-Kosten waveguide propagation model.

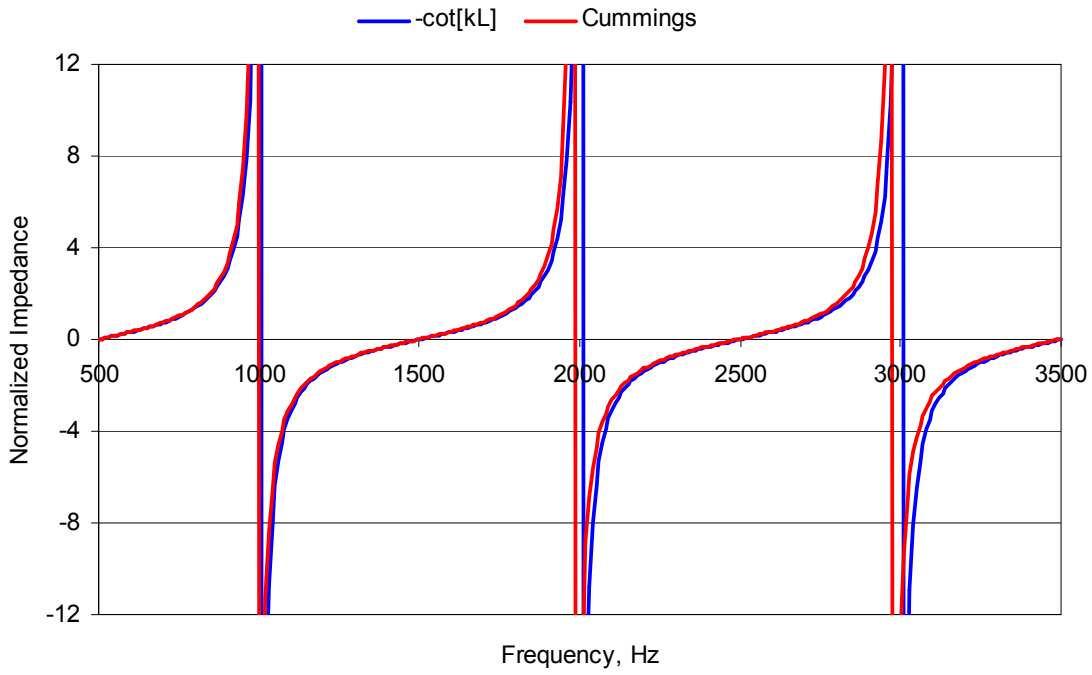

Figure 15. Reactance shift as calculated from Cummings, lossless, modal model for 180° bend compared to simple 1-D, -cot[kL] model – suggesting that for 500 Hz ≤ ϕ ≤ 3500 Hz, bend has minimal effect on channel reactance.

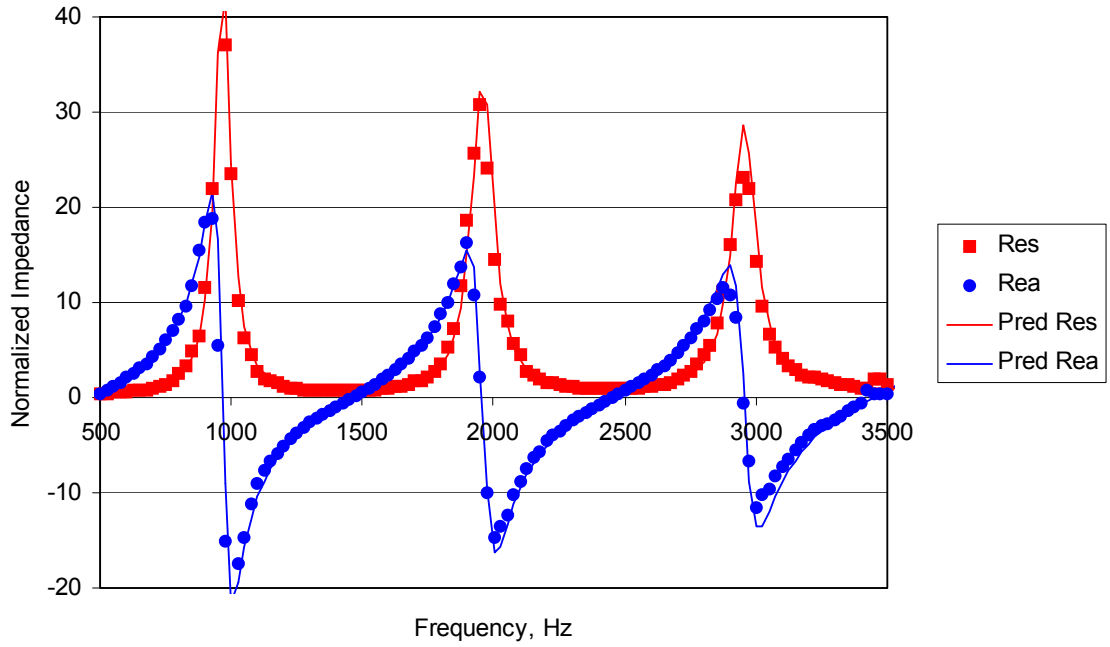

Figure 16. Normalized impedance for Configuration-C1 (straight channels), 120dB.

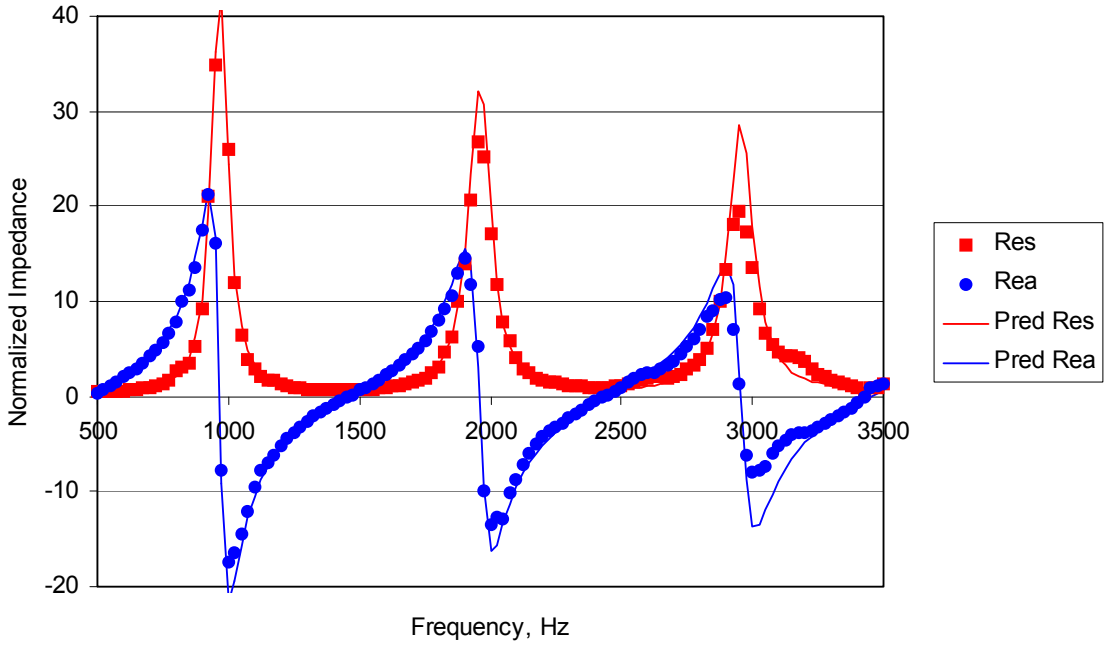

Figure 17. Normalized impedance for Configuration-C2 (45^{o} skew), 120dB.

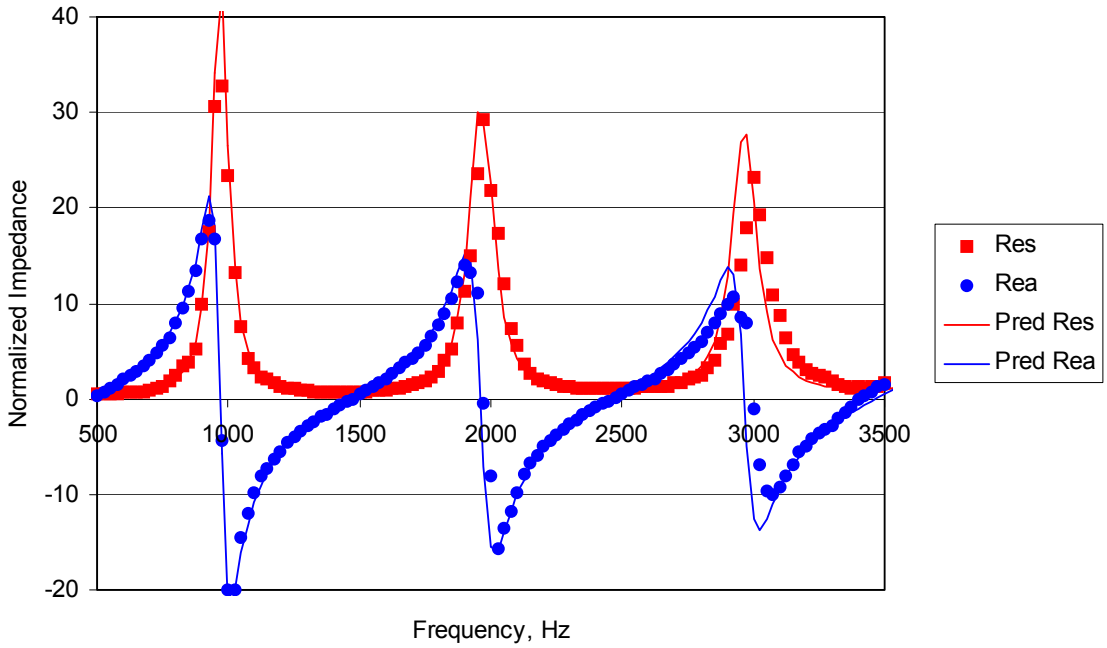

Figure 18. Normalized impedance for Configuration-C3 (90^{o} bend), 120dB.

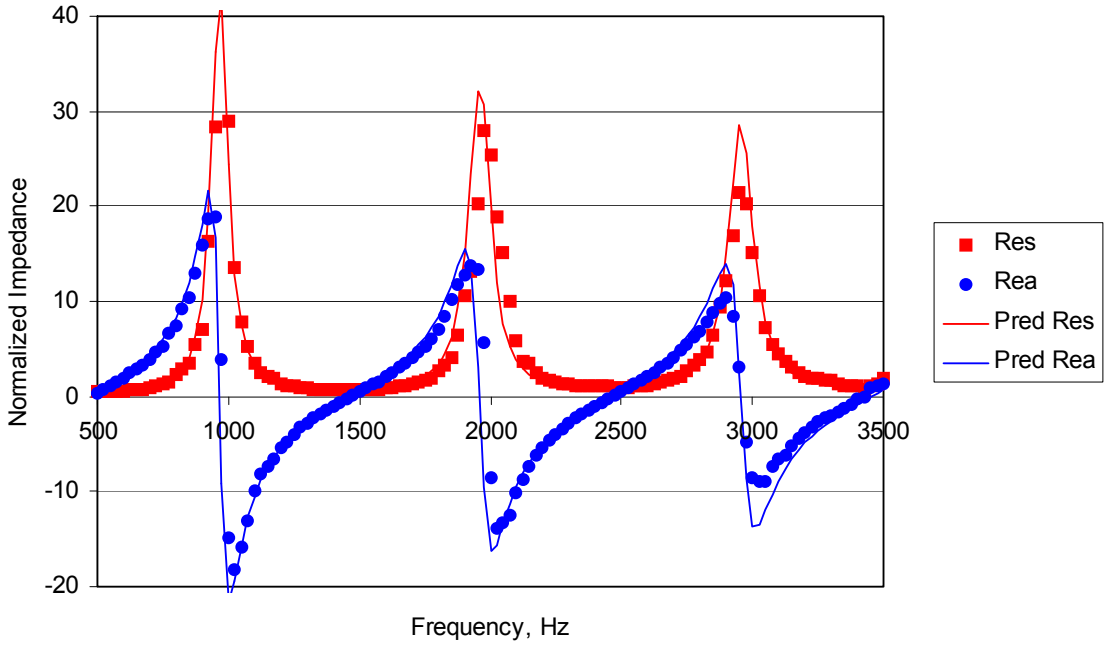

Figure 19. Normalized impedance for Configuration-C4 (double 90° bends), 120dB.

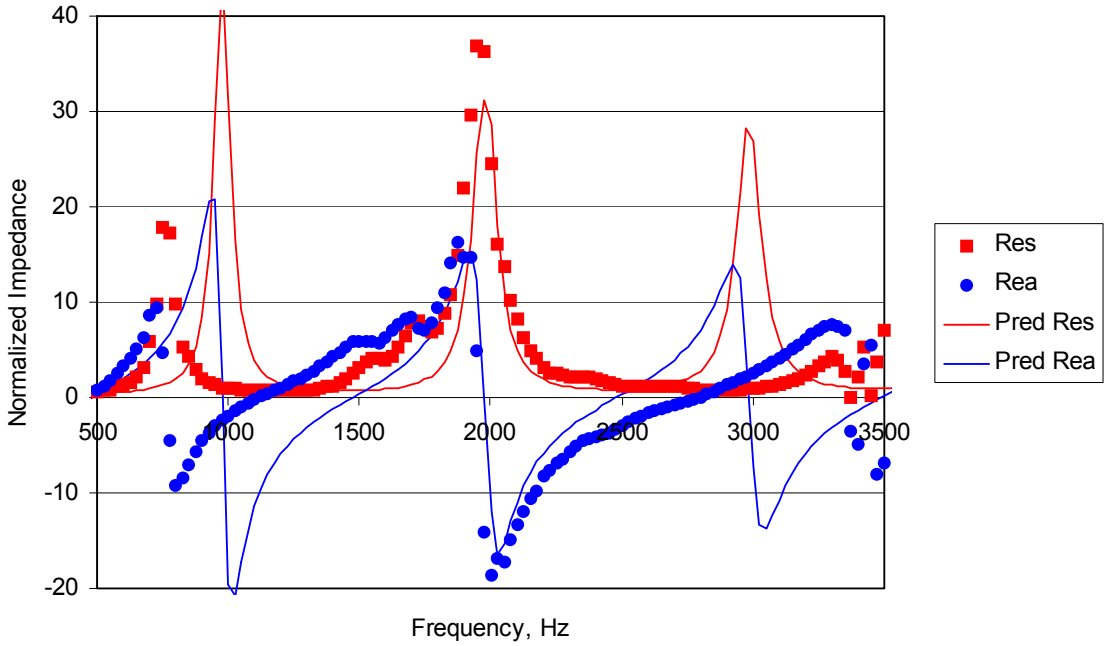

Figure 20. Normalized impedance for Configuration-C5 (180° bend), 120dB.

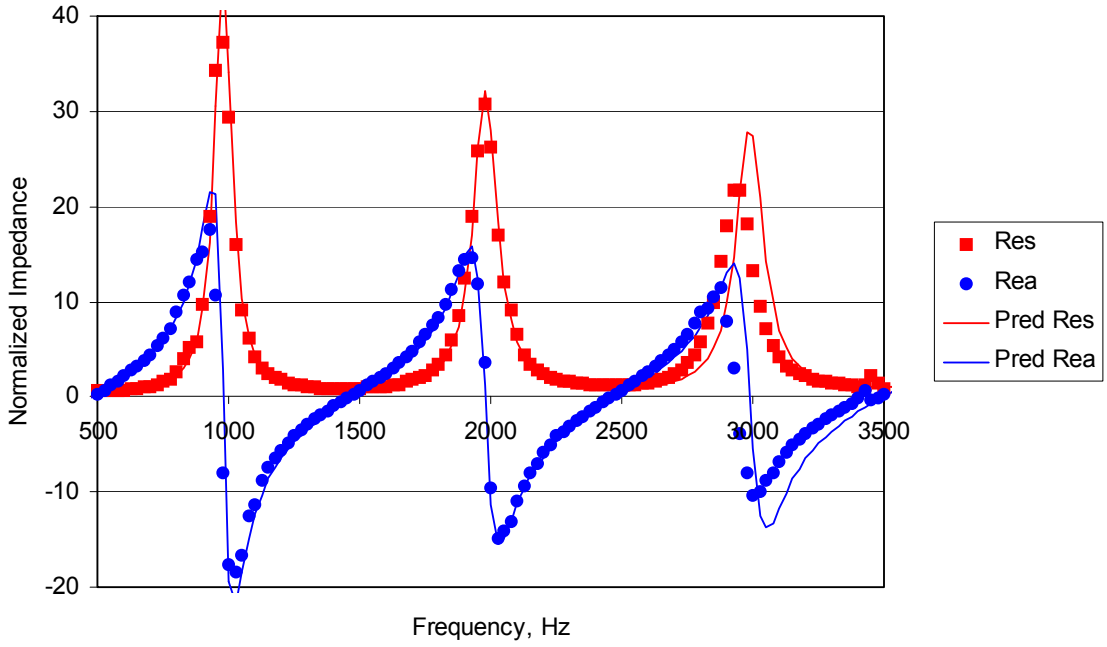

Figure 21. Normalized impedance for Configuration-C6 (partitioned 180° bend), 120dB.

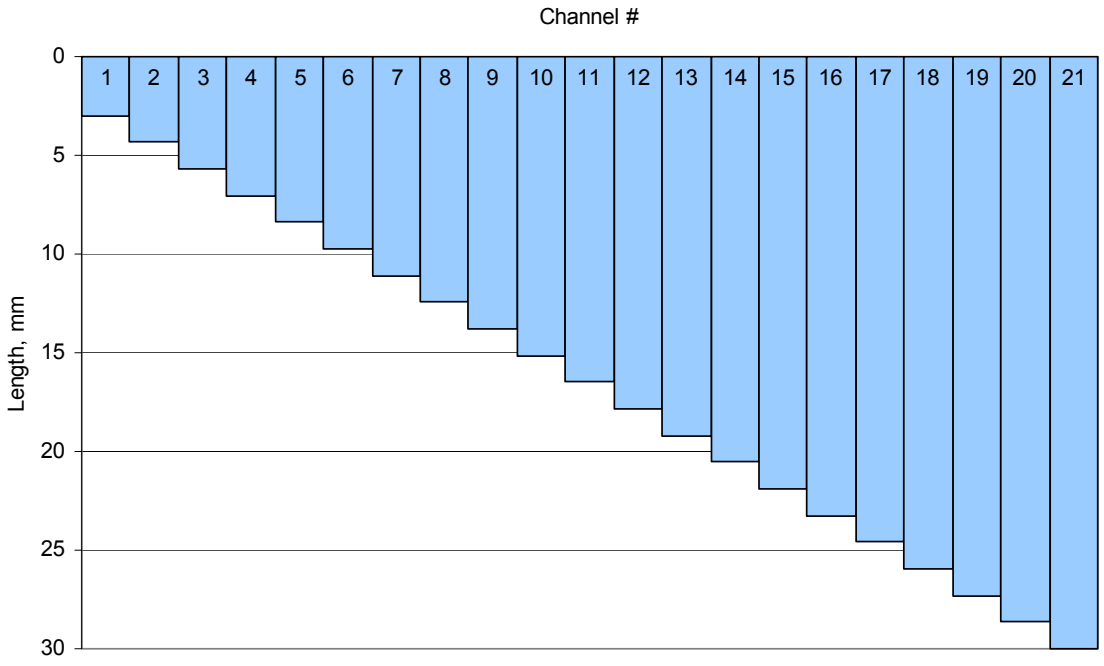

Figure 22. A linear stepped array of 21 resonator channels ranging from 3 to 30 mm in depth.

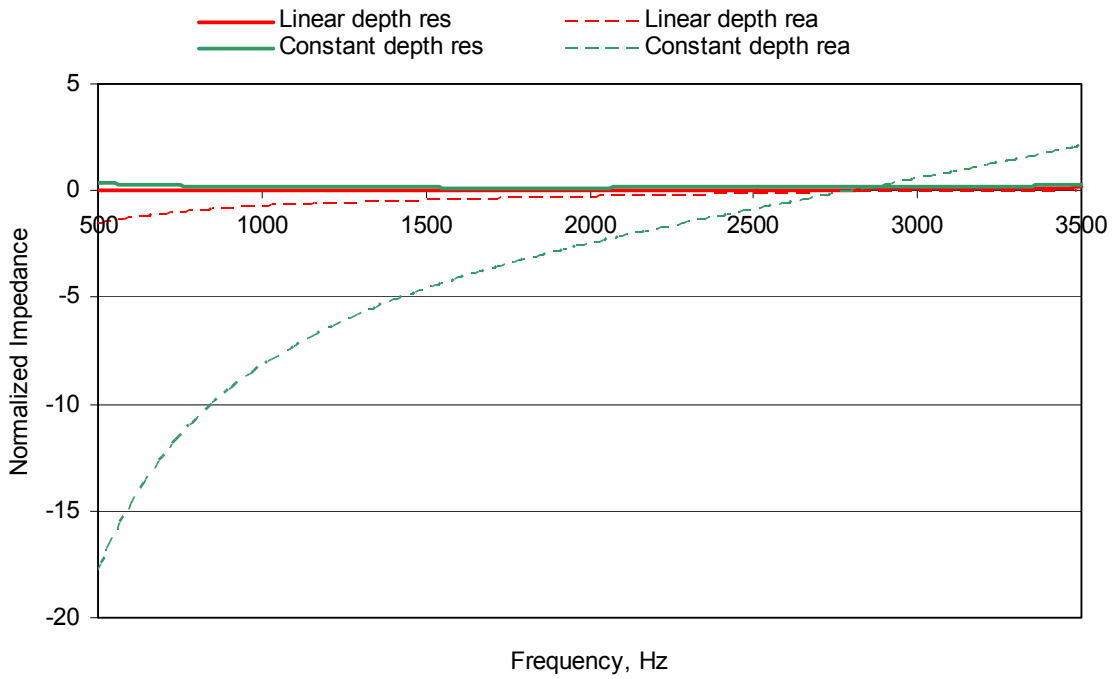

Figure 23. Comparison of impedance spectra for a constant depth and linearly stepped array of 21, parallel channels.